RevMexAA (Serie de Conferencias), **29**, 1–8 (2007)

SCIENCE WITH CANARICAM

Charles M. Telesco[1]

RESUMEN

CanariCam es la cámara multi-modal en el IR-intermedio que se ha desarrollado en la Universidad de Florida para usarse en el Gran Telescopio CANARIAS (GTC). CanariCam se encuentra en la fase de pruebas intensas de laboratorio en preparación para la pruebas formales de aceptación a verificarse en la Universidad de Florida en la primavera de 2007. CanariCam será enviada al GTC en el verano del 2007, y estará disponible para las observaciones científicas de que se iniciarán el Día-1. El instrumento está operando bien, y no anticipamos ningun obstáculo que nos impida tener lista CanariCam para el Día-1 del GTC.

ABSTRACT

CanariCam is the multimode mid-IR camera being developed at the University of Florida for use at the Gran Telescopio CANARIAS (GTC). CanariCam is undergoing extensive laboratory tests in preparation for formal laboratory Acceptance Tests to be held at the University of Florida in spring 2007. CanariCam will be shipped to the GTC in summer 2007, and it will be available for Day-1 science observing. It is functioning well, and we do not anticipate obstacles to our having CanariCam ready for the GTC on Day-1.

Key Words: **INFRARED: GENERAL — INSTRUMENTATION: SPECTROGRAPHS — INSTRUMENTATION: POLARIMETERS**

1. OVERVIEW

CanariCam is optimized for use at 8 - 25 μm, the so-called mid-IR spectral region, but it is useful for certain key engineering observations down to about 2 μm. The goal has been to provide the GTC astronomy community with an outstanding "workhorse" multi-mode instrument for use in the atmospheric windows near 10 μm (extending from about 8 to 14 μm) and 20 μm (extending from 16 to roughly 25 μm). The detector is an arsenic-doped silicon, blocked-impurity-band (BIB, or IBC) device from Raytheon, with peak quantum efficiency (QE) in the 8 - 25 μm region and a rapid decrease in QE at longer wavelengths. The detector array contains 240×320 pixels, each $0.08''$, which provides a field of view on the sky of $19'' \times 26''$. The diffraction point spread function is Nyquist-sampled at 8 μm (two pixels per resolution element). The CanariCam science modes available are standard imaging, slit spectroscopy, dual-beam polarimetry, and coronagraphy. All modes are available for use in the 10 μm region, but only imaging and spectroscopy will be available at 20 μm on Day-1. Additional technical information about CanariCam is available in Telesco et al. (2003).

[1]Department of Astronomy, University of Florida, 211 Bryant Space Science Building, Gainesville, Fl 32608, USA (telesco@astro.ufl.edu).

CanariCam will address a broad range of scientific problems. Astronomical bodies at temperatures of 100-1000 K emit significant mid-IR radiation. Of particular importance are the ubiquitous small solid particles—dust—that absorb radiation at virtually any wavelength and transform it into infrared, submillimeter, or millimeter radiation. Mid-infrared continuum emission from the dust is diagnostic of the properties of a great variety of astrophysical objects, including planets, circumstellar disks, star-forming regions, and starburst and active galactic nuclei. With multi-wavelength mid-IR imaging, one can locate energy sources that power often enormous luminosities, trace the distributions of dust particles and their temperatures, and determine how UV and optical radiation, which heats the dust, propagates throughout the infrared-emitting regions. The coronagraphic mode is ideally suited to the investigation of sub-stellar objects in close proximity to 'parent' stars. Finally, polarimetric observations allow detailed mapping of the magnetic alignment of dust particles in objects such as circumstellar disks, young stars and active galaxies. Below, I provide additional comments about each mode of operation in the context of examples of the science for which CanariCam will be a valuable tool of exploration. My goal is to provide examples that illustrate CanariCam's anticipated capabilities, rather than to review the field of mid-IR astronomy. Therefore, for convenience, I

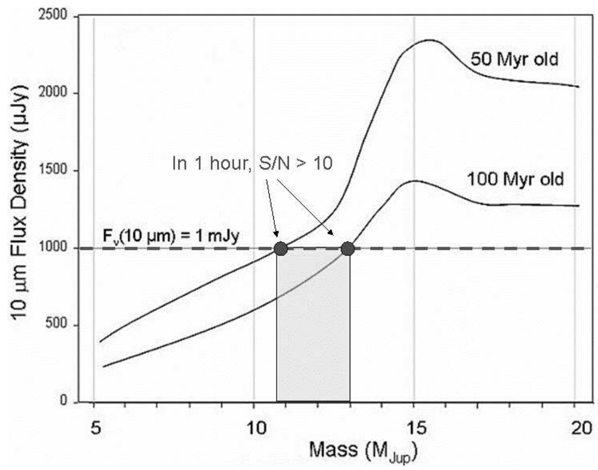

Fig. 1. Anticipated CanariCam 10 μm sensitivity for young free-floating brown dwarfs at 20 pc.

have taken the liberty of drawing most of these examples from the research of my colleagues and me, even though much interesting mid-IR research is being carried out by others. In addition, because it is very similar in design to CanariCam (which, however, has additional modes), I present several results from the Florida-built instrument T-ReCS in use at Gemini South, since they are the best examples of what CanariCam will be capable.

2. IMAGING

Mid-IR imaging is considered to be the fundamental science mode for CanariCam, and implementation of the other modes cannot compromise the imaging performance. At an excellent site like Roque de los Muchachos, the mid-IR point spread function will be dominated by diffraction, not seeing, and the 10 and 20 μm resolutions ($\sim \lambda$/D) will often be as good as 0.2$''$ and 0.4$''$, respectively. Because the design of CanariCam is based on the design of the Florida-built instrument T-ReCS, which is now fully operational at Gemini South in Chile, we have a good idea of how sensitive CanariCam will be-it will be very good (Bouchet et al. 2004)! In the broadband 10 μm filter (the N band) on a very good night, we estimate a point-source photometric sensitivity of 0.06 mJy, which is the 1σ noise level achieved in 1 hour of chopped (on plus off source) integration time. On somewhat lower quality nights (i.e., higher background and sky noise, lower transmission), the sensitivity will be worse, but this value gives a good idea of what is possible. Generally, because of much lower atmospheric transmission and correspondingly higher background at longer wavelengths, the 20 μm sensitivity is about ten times worse than at 10 μm.

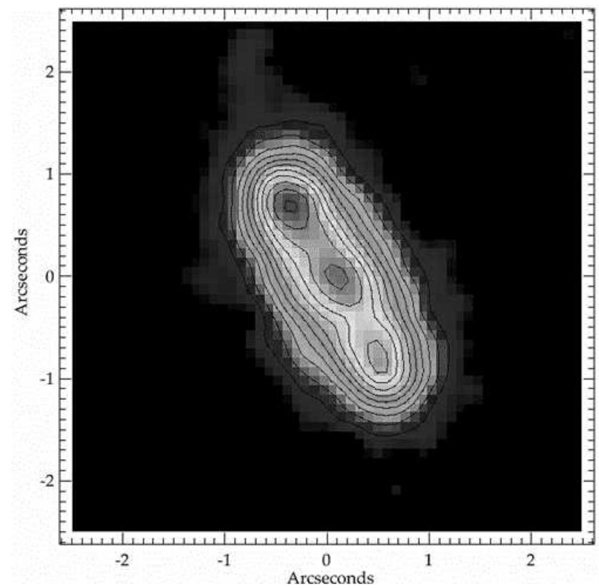

Fig. 2. T-ReCS image at 18 μm of the edge-on disk of HR 4796A (Fisher et al. 2007).

To illustrate the science enabled by this sensitivity, consider the detection limit for “free-floating” brown dwarfs (BDs). Based on model atmospheres (Hubbard, Burrows, & Lunine 2002), we show in Figure 1 the expected 10 μm flux densities for young (50 and 100 Myr) BDs and giant planets located at 20 pc. The shaded area indicates that young BDs with masses as low as 11-13 M(Jup), where M(Jup) is Jupiter's mass, can be detected with a S/N $>$ 10 in reasonable integration times. CanariCam will permit exploration of BDs with a broad range of masses (Sterzik et al. 2004) and ages, including those with masses near the BD-exoplanet boundary.

The outstanding angular resolution of CanariCam can permit fruitful exploration of the detailed properties of many types of astronomical sources. In the area of disk research, CanariCam will be used to search for structure in circumstellar disks where planets are forming or have formed. Planets embedded in both primordial and debris disks influence the disk morphology, and we are thereby able to infer properties of the embedded planetary systems. For example, the well known edge-on disk orbiting the star HR 4796A, which was discovered at 10 μm (Jayawardhana et al. 1998; Koerner et al. 1998), shows strong asymmetries (Telesco et al. 2000). A new image at 18 μm, obtained with T-ReCS at Gemini South, is shown in Figure 2 (Fisher 2007). The IR emission arises from starlight-heated dust particles. The central clump coincides with the star,

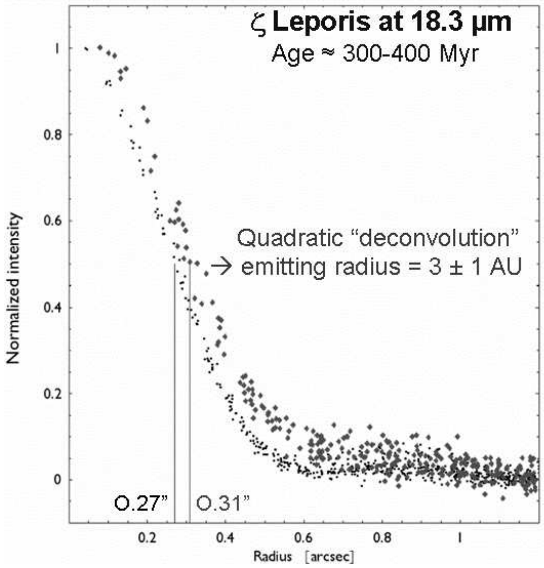

Fig. 3. Data profile of disk of the star ζ Lep, at right, with a point source, at left (Moerchen et al. 2007).

and the two outer clumps are ansae associated with the ring. However, the NE lobe is brighter than the SW lobe. This may be related to planetary perturbations (Liou & Zook 1999), or, as suggested for β Pic, it may represent the asymmetric distribution of recently created debris associated with the collisional breakup of a large body (Telesco et al. 2005). These and other possibilities can be examined with detailed multi-wavelength imaging, a powerful mode of CanariCam.

Even unresolved or barely resolved sources can be of deep interest, and CanariCam on the superb 10-m GTC will provide the best combination of mid-IR resolution and sensitivity of any groundbased observatory. The 230 Myr-old A star ζ Leporis illustrates this well (Figure 3). This star has a bright disk which was unresolved until we (Moerchen et al. 2007) used T- ReCS to show that the disk has a radius of about 3 AU, comparable in size to our solar system's asteroid belt as had been previously surmised (Chen & Jura 2001). This appears to be the first-ever resolution of an asteroid-belt around another star, and this object may be the archetype for a new class of disk, the asteroid-belt analog. Another excellent example of the power of high angular resolution is the imaging of the active galactic nucleus (AGN) of the Circinus galaxy, which Packham et al. (Packham et al. 2005) showed must be smaller than $0.2''$, or 4 pc, at 10 μm, a size that is a challenge to our understanding of AGNs in the context of the unified model.

TABLE 1

CANARICAM SPECTROSCOPY

Grating	Spectral Range (μm)	R
Lo-Res-10	8-14	175
Lo-Res-20	16-26	120
Hi-Res-10	8-14	1310
Hi-Res-20	16-26	890

3. SPECTROSCOPY

The CanariCam spectrometer sub-system follows that of the Czerny-Turner layout using any one of four classical plane gratings installed on a turret. The general grating properties are listed in Table 1. The indicated diffraction-limited resolving powers are approximate, with final values to be determined during the laboratory tests. By assuming that the limiting fluxes scale as $R^{1/2}$, where $R \equiv \lambda/\Delta\lambda$, we can estimate sensitivities in this mode from the broadband sensitivities. The approximate Lo-Res-10 and Hi-Res-10 continuum point-source sensitivities (1σ, 1 hour, chopped integration) are 1 mJy and 3 mJy, respectively, and the corresponding line sensitivity in the 10 μm region is about 10^{-18} Wm^{-2}.

Among the exciting problems that can be addressed with CanariCam's spectroscopic mode is the study of the mineralogy and composition of large molecules and solid particles in many types of astrophysical environments. By determining the 10 μm spectrum at many locations very near the Circinus AGN, Roche et al. (2006) were able to show (Figure 4) that features associated with polycyclic aromatic hydrocarbon (PAH) molecules are weaker at the AGN core than in surrounding regions, presumably indicating that the AGN core is embedded in a much more extended region of star formation also manifested by a silicate absorption feature. Silicate minerals exhibit broad silicate features at both 10 and 20 μm, which can be in either absorption or emission. The shapes of these features in many types of astrophysical sources differ from that of the general interstellar medium. For example, the disks of Herbig Ae/Be stars (pre-main-sequence A stars), as a class exhibit a rich variety of shapes of the 10 μm emission feature, some of which are more peaked, like that of amorphous silicate dust in the ISM, some of which are nearly flat-topped, and some of which have sub-structure indicative of crystalline components (van Boekel et al. 2003). This variety may represent evolutionary trends or other fundamental properties of the sources, but their study offers the opportunity

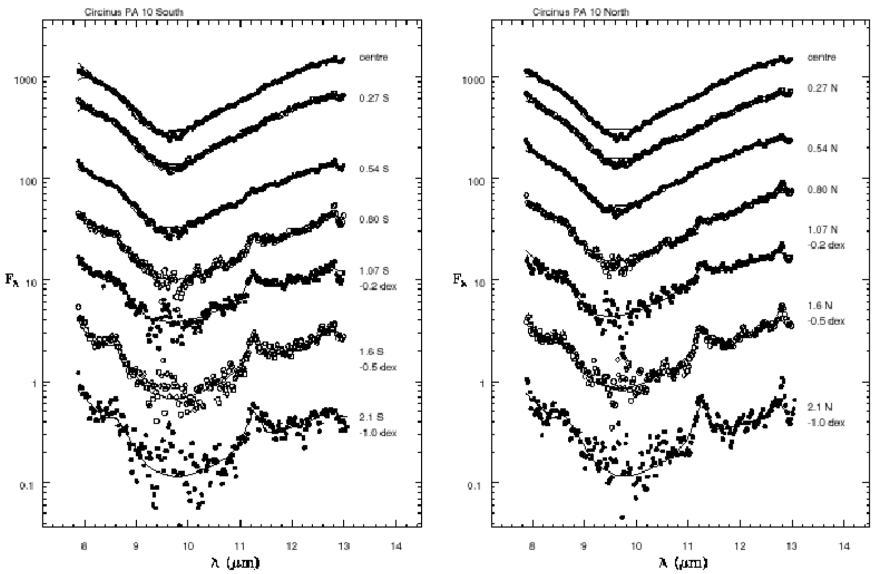

Fig. 4. Spectra at 10 μm of the silicate feature at various locations near the Circinus AGN (Roche et al. 2006).

to probe the solid particles in complex environments, including those where planets are forming. As an illustration, we show in Figure 5 silicate spectroscopy of the class 0/1 protostars SVS20 N & S located at 250 pc. These deeply embedded stars, which are only about 0.1 Myr old and separated from each other by about 1″, exhibit very different silicate features. One (SVS20-S) is in emission, and the other is in absorption (Ciardi et al. 2005). We do not yet know why the features from these two coeval stars appear so different, but clearly this spectral information provides one basis for detailed modeling of the radiation transfer in this complex environment. Interestingly, they also show evidence for the crystalline sub-structure, which therefore can appear very early in the evolution of the circumstellar dust.

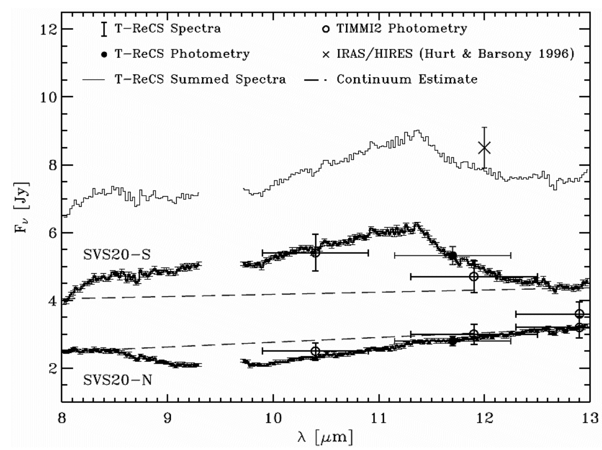

Fig. 5. Silicate emission features in SVS20-N & S, as well as (top) the composite spectrum (Ciardi et al. 2005).

A variety of diagnostic emission lines are also available in the mid-IR spectral region. These include the H recombination lines at 12.4 μm (7-6) and 11.3 μm (9-7) and key fine-structure lines, most importantly the [ArIII] 9.0 μm, [SIV] 10.5 μm, and [NeII] 12.8 μm lines. While the CanariCam spectral resolutions are not high enough to determine much dynamical information from the line spectra, they can tell us much about the distribution of excitation in interesting astrophysical environments. For example, the indicated fine-structure lines are a powerful probe of the UV continuum and therefore the star-forming complexes in starburst galaxies. Due to their inherently high extinction, these regions are often heavily obscured visually and even in the near-IR, so these mid-IR lines are sometimes the only way to accurately assess the magnitude and distribution of central star formation. The classic case is M82, which has the added problem of being edge-on, which greatly increases the line-of-sight extinction. Mid-IR continuum and line imaging is one of the few ways to probe this archetypal galaxy's starburst core (Jones & Rodríguez-Espinosa 1984; Achtermann & Lacy 1995).

4. POLARIMETRY

CanariCam will have the first dual-beam mid-IR polarimetric mode. Initially it will only be used in the 10 μm region, but, at a later date, it will be possi-

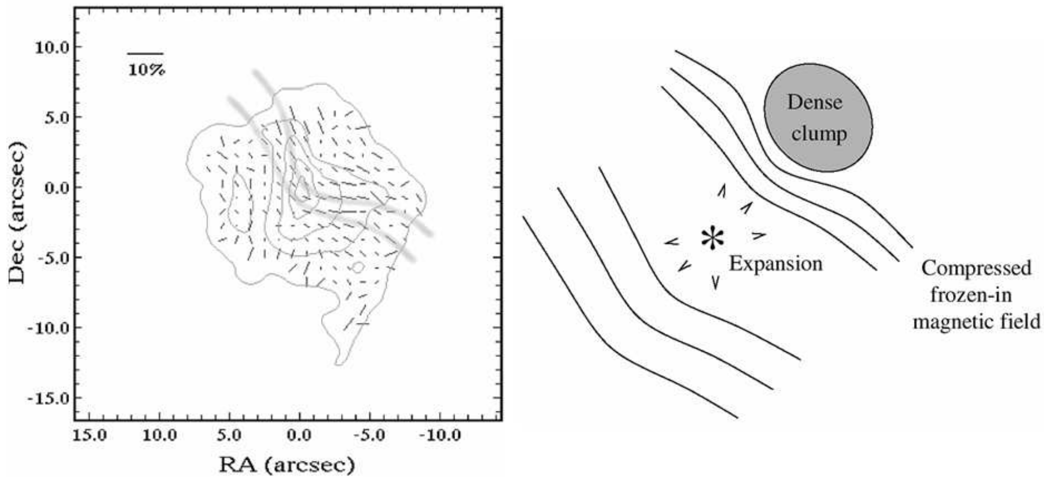

Fig. 6. Mid-IR polarization of the compact HII region G333.6-0.2 (Fujiyoshi et al. 2001). Left panel: absorption-subtracted 12 μm polarization vectors, rotated by 90°. Right panel: the inferred magnetic field structure and its relationship to the expanding wind and adjacent clump compression.

ble to extend this capability to the 20-micron region with the implementation of the corresponding half-wave plate. Since this is a very unique capability, the design warrants further description. The key components of the polarimetric design are: (1) a cooled, rotatable (sulphur-free) CdSe half-wave plate (HWP, retarder) within the cryostat located just upstream from the telescope focal plane; (2) a focal-plane mask at the telescope focal plane; and (3) a (Sulphur-free) CdSe Wollaston prism (analyzer). The HWP will be rotated sequentially to four different discrete orientations (0, 22.5, 45, and 67.5 degrees), with images being taken at each HWP orientation. The Wollaston prism, which, to our knowledge, is the largest ever built, is inserted into the beam on a slide, and produces an angular separation between the orthogonally polarized states, thereby producing two beams, the so-called o and e rays, which results in two images of the object being formed on the detector. This simultaneous measurement of the ordinary (o) and extraordinary (e) rays not only increases observational efficiency but also minimizes effects of seeing and changes in atmospheric transparency. When using a dual-beam analyzer, a special focal plane mask is required so that extended objects can be observed without overlap of the orthogonally polarized images. The separation of beams is usually a compromise between possible optical aberrations produced for large separations and cross-talk for too small a separation. Large separations are convenient, since extended objects may be fully covered by one of the mask gaps, and observations can be made with a single setting of the telescope.

TABLE 2

CANARICAM POLARIMETRIC SENSITIVITY

$F_\nu(10\mu m)$	P (%)	1σ(%)
10 mJy	1.5	0.5
50 mJy	0.3	0.1
165 mJy	0.10	0.03

For a dual-beam polarimeter, an absolute uncertainty in the degree of polarization of 0.5% requires a S/N ratio of ∼300:1 in total flux. For the source-limited case this corresponds to 8×10^4 photons or 4×10^4 per Stokes parameter. Thus, with a dual-beam system the accuracy obtained is a function of photon numbers only, and accurate polarimetry of bright sources can be carried out during observing conditions that are too poor for almost any other type of quantitative observation. CanariCam's polarimetric mode will be able to measure degrees of polarization as small as ∼0.1% in both the 10-micron atmospheric window. Table 2 gives an indication of the expected CanariCam polarimetric sensitivities. The table indicates the level of polarization P that can be measured with S/N ≈ 3 for a source with 10 μm flux density F_ν.

CanariCam will be a pioneering instrument in mid-IR polarimetric studies. While not entirely negligible in the mid-IR, polarization due to scattering from dust, which is an important polarization process at shorter wavelengths, is expected in most astrophysical environments to be swamped by transmission through, and emission by, populations of elongated particles. An elongated dust particle both absorbs and emits the electric-field component parallel to its long axis. For a population of elongated grains that are absorbing radiation from a more distant mid-IR emitting source as well as emitting their own mid-IR radiation, multi-wavelength mid-IR polarimetric measurements can permit one to distinguish the absorbed and the emitted components (Aitken et al. 2004). As the pioneers of this field such as Dave Aitken and Jim Hough have demonstrated, exciting science is possible with mid-IR polarimetry. Because magnetic fields align elongated grains, the resultant mid-IR polarization distribution that we may determine for young circumstellar disks has the potential to provide tremendous insight into the distribution of the magnetic fields in these environments (Aitken et al. 2002). These magnetic-field distributions must play a critical role in the formation of planets in these systems. While progress is being made (Aitken et al. 2002) in modeling the expected mid-IR polarization distribution for a specific magnetic-field configuration, much work in this area needs to be done. Hopefully, the CanariCam polarization mode will serve as a great stimulus to this important area of research.

As an excellent example of the value of mid-IR polarimetry, consider the study by Fujiyoshi et al. (2001) of the compact HII region G333.6-0.2. Their multi-wavelength polarimetry across the 10 μm region permitted them to separate the emission and absorption components. By considering the polarized emission, they then inferred the distribution of the magnetic field (Figure 6). They conclude that the magnetic field curvature and strength is well explained by a model in which the magnetic field has been compressed by the wind from a young star, which in turn has led to the compression of adjacent cloud material to produce a density enhancement that may in fact be a future region of star formation. This beautiful piece of work shows the insight that is uniquely provided by polarimetric studies.

5. CORONAGRAPHY

For stars observed in the mid-IR, thermal background emission from the sky and the telescope will be many orders of magnitude larger than the stellar flux. By the use of chopping and nodding techniques, however, it is possible to remove this background at levels approaching one part in a million. Once the background has been removed, the focal plane intensity will be dominated by the stellar point spread function (PSF), the wings of which can be

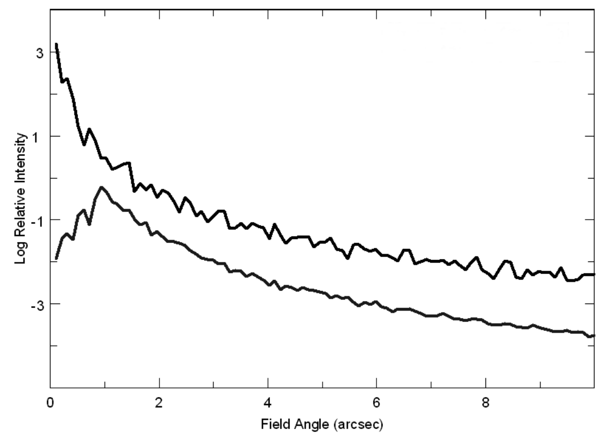

Fig. 7. Azimuthal averages of the point-spread function with and without the coronagraphic mode.

thought of as a "halo" arising from diffracted and scattered light. The key motivation for the coronagraphic mode is to suppress the stellar halo, or PSF wings, to allow circumstellar searches for disks and faint companions. An important goal of an effective coronagraphic mode is to minimize residual diffractive structure in the focal plane with minimum losses in field of view and throughput.

To illustrate key performance advantage of the CanariCam coronagraphic mode, we consider the case of good atmospheric conditions at an observing wavelength of 10 μm defined by a Fried scale length of order the size of the aperture (10-m) and an outer scale twice the size of the aperture (20-m). These parameters define peak atmospheric conditions. We assume that the star is occulted in the telescope focal plane by a hard-edged (top-hat), low reflectivity circular occulting mask 0.83 arcsec in radius. In Figure 7 we show a plot of the log of the azimuthally averaged intensities as a function of the distance from the star. The top line represents the stellar image PSF for no coronagraphic masks. The lower line represents the stellar image for the occulting mask and a Lyot mask that has a serrated and hex-shaped outer mask that matches the pupil shape, including masks that block the secondary-mirror spiders.

We find that one achieves a suppression ratio of about an order of magnitude. The baseline CanariCam coronagraphic mode employs a rotating Lyot stop and maximizes the throughput but provides some leeway for the operational complexity anticipated as the mask rotates. The basic design, then, consists of: (1) a hard-edged (top hat), low-reflectivity, focal-plane (i0) mask 0.83 arcsec in radius; (2) a hard-edged, rotating Lyot stop with a

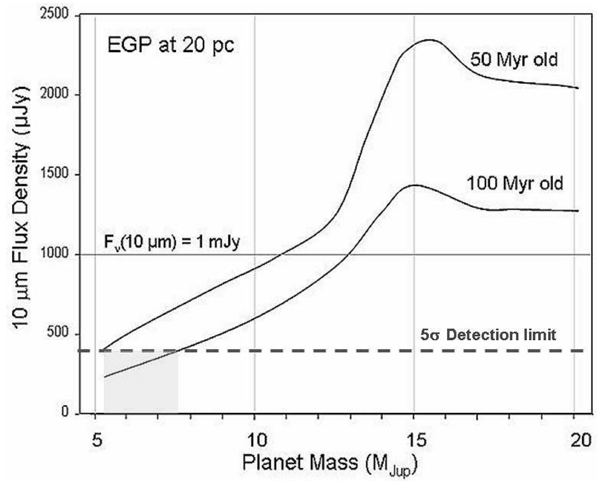

Fig. 8. The horizontal dashed line indicates the detection limit of CanariCam in the coronagraphic mode for you giant exoplanets.

spider mask with widths 20 times the spider-image width. The rotating Lyot stop is dodecagonal (12-sided) and scaled from the input pupil so that the outer dodecagonal edge is 90% the size of the image of the original. A central hard-edged, circular mask blocks out the secondary mirror/obscuration; that mask is 140% the size of the image of the original. The total throughput of the Lyot stop is 66%.

Based on experience at shorter wavelengths, the sensitivity of the coronagraphic mode is expected to be dominated by systematic effects. Consider the following. To detect a faint companion around an occulted star one must subtract from the program object's observed intensity profile that of a comparison star observed in the same coronagraphic configuration. This subtraction of the normalized profile can be made to an m (fractional) level of accuracy (i.e., probable error equals m times the intensity at the radius where the companion may be located). Experience in the near-IR suggests that m is approximately 0.1-0.2. Therefore, if the coronagraphically suppressed profile is about ten times fainter than the standard (non-coronagraphic) imaging profile, the absolute error in the measured flux is about ten times smaller than for standard imaging.

In some cases this permits one to be background-limited rather than profile-subtraction-limited. Assume, for example, that m=0.2. For 1 h of chopped integration for the program object and another 1 h for the profile object, the 5σ detection limit, at a companion located 20 AU (1″) from a Sun-like star 20 pc away, is about 0.4 mJy in coronagraphic mode compared to 1 mJy in the standard imaging mode. As illustrated in Figure 8, this seemingly modest gain now permits one to potentially detect young giant exoplanets with masses smaller than 10 M(Jup).

CanariCam will be a tremendous resource for the GTC community. I hope I have been able to convey at least some sense of the exciting science that will be possible, and I thank you very much for giving me the wonderful opportunity here in beautiful Barcelona to tell you about CanariCam.

It is with pleasure that I acknowledge my fellow team members (past and present) of the CanariCam instrument team who have worked, and continue to work, so hard to bring CanariCam to the GTC: Chris Packham, Jeff Julian, Kevin Hanna, Frank Varosi, Roger Julian, David Hon, Craig Warner, Dave Ciardi, Christ Ftaclas, Jim Hough, Margaret Moerchen, Robert Pia, Jim French, Glenn Sellar, and Mark Kidger.

REFERENCES

Achtermann, J., & Lacy, J.1995, ApJ, 439, 163
Aitken, D. K., Hough, J. H., Roche, P. F., Smith, C. H., & Wright, C. M. 2004, MNRAS, 348, 279
Aitken, D. K., Efstathiou, A., McCall, A., & Hough, J. H. 2002, MNRAS, 329, 647
Bouchet, P., DeBuizer, J. M., Suntzeff, N. B., Danziger, J., Hayward, T. L., Telesco, C. M., & Packham, C. C. 2004, ApJ, 611, 394
Chen, C., & Jura, M.2001, ApJ, 560, L171
Ciardi, D. R., Telesco, C. M., Packham, C., Gomez-Martin, C., Radomski, J. T., De Buizer, J. M., & Phillips, C. J. 2005, ApJ, 629, 897
Fisher, R., Telesco, C., Knights, S., Volk, K., & Packham, C. 2007, in preparation
Fujiyoshi, T., Smith, C., Wright, C., Moore, T., Aitken, D., & Roche, P. 2001, MNRAS, 327, 233
Hubbard, W., Burrows, A., & Lunine, J. 2002, ARA&A, 40, 103
Jayawardhana, R., Fisher, S., Hartmann, L., Telesco, C., Piña, R., & Fazio, G. 1998, ApJ, 503, L79
Jones, B., & Rodríguez-Espinosa, J. M. 1984, ApJ, 285, 580
Koerner, D., Ressler, M., Werner, M., & Backman, D. 1998, ApJ, 503, L83
Liou, J., & Zook,H. 1999, AJ, 118, 580
Moerchen, M., Telesco, C., Packham, C., & Kehoe, T. 2007, ApJ, 655, L109
Packham, C., Radomski, J. T., Roche, P. F., Aitken, D. K., Perlman, E., Alonso-Herro, A., Colina, L., & Telesco, C. 2005, ApJ, 618, L17
Roche, P. F., Packham, C., Telesco, C. M., Radomski, J. T., Alonso-Hererro, A., Aitken, D. K., Colina, L., & Perlman, E. 2006, MNRAS, 367, 1689

Sterzik, M., Pascucci, I., Apai, D., van der Bliek, N., & Dullemond, C. 2004, A&A, 427, 245
Telesco, C. M., et al. 2000, ApJ, 530, 329
Telesco, C. M., et al. 2003, Proc. SPIE, 4841, 913
Telesco, C. M., et al. 2005, Nature, 433, 133
van Boekel, R., Waters, L., Dominik, C., Bouwman, J., de Koter, A., Dulllemond, C., & Paresce, F. 2003, A&A, 400, L21